Desalination 311 (2013) 1–15

Contents lists available at SciVerse ScienceDirect

Desalination

journal homepage: www.elsevier.com/locate/desal

Optimization of Multi-Effect Evaporation desalination plants

Paula Druetta, Pio Aguirre, Sergio Mussati *

INGAR Instituto de Desarrollo y Diseño (CONICET-UTN), Avellaneda 3657 (S3002GJC) Santa Fe, Argentina

HIGHLIGHTS

- A simplified but accurate enough mathematical model of MEE is presented.
- The flow-patterns for the distillate and the vapors were optimization variables.
- A novel structure was found and compared with the conventional one.
- The novel structure has a better performance than the conventional structure.
- Uniform and non-uniform heat transfer area distributions were also analyzed.

ARTICLE INFO

Article history:
Received 8 September 2012
Received in revised form 25 October 2012
Accepted 26 October 2012
Available online 20 December 2012

Keywords:
Multi-Effect Evaporation system
Optimization
Non-linear programming (NLP)

ABSTRACT

This paper focuses on the mathematical modeling and optimization of Multi-Effect Evaporation plants (MEE). A simplified and detailed enough model to accurately predict the MEE system performance is presented. The model is highly nonlinear and it is based on mass and energy balances which are derived from a superstructure. The superstructure involves several process configurations which have to be simultaneously optimized to determine the best stream flow-patterns (synthesis), the size of each evaporation effect (sizing) and the operating conditions of the whole process. Beside the conventional configuration, the model also includes different alternative flow-patterns for the distillate and the vapor streams. An equation-oriented environment was selected to develop and implement the model, allowing different application instances, such as simulation, sensitivity analysis and optimization, to be easily performed.

Simulation results have shown a good agreement with realistic design data and other authors' results. A ranking of the model parameters is presented according to their impact on the heat transfer area. Moreover, optimization results showed that the modification of the flow patterns improve the process performance, reducing the process specific total heat transfer area in about 5% compared to the optimal value of the conventional case.

1. Introduction

Seawater desalination has played and it will still play an important role in the future in the provision of fresh-water around the world. There exist several desalination technologies and, depending on the separation mechanism used in each one of them, they can be classified into three major groups: a) Heat consuming or thermal processes: Multi Stage Flash (MSF) and Multi-Effect Evaporation (MEE) systems, Vapor Compression (VC) and b) Power consuming or membrane processes: Reverse Osmosis (RO), Electrodialysis (ED) and c) Hybrid processes: which result from the combination of a) and b). The thermal processes are particularly preferred in large-scale seawater desalination plants while ED and RO systems are more convenient for irrigation and industrial use. The main difference between MSF and MEE systems lies in the way of evaporation and heat transfer.

Studies about seawater desalination processes have been around since the end of the 18th century [1]. Desalination received significant attention approximately in 1960 and it started to emerge as a larger scale process [2]. Despite that significant progress on desalination processes was made since 1960s, technological and research efforts are still required to improve the system's efficiency and reduce water production cost. One of the research areas, which will be specifically addressed in this paper, is the modeling, simulation and optimization of MEE units using advanced mathematical programming tools. They can be effectively used to gain insights and identify trade-offs between the process variables which help to determine feasible and optimal process designs. Certainly, process alternatives and modifications can be easily evaluated by reliable mathematical models in short times.

A great number of articles dealing with the simulation and parametric optimization of thermal desalination processes have been published [3–15]. Certainly, a wide variety of models, ranging from steady-state to dynamic models, have been developed in order to analyze the performance of different configurations of MEE plants. The majority of the simulation models have been implemented in process simulators as in-house computer codes. The simulation programs have been used to

* Corresponding author. Tel.: +54 342 453 5568; fax: +54 342 455 3439.
E-mail addresses: pauladruetta@santafe-conicet.gov.ar (P. Druetta), paguir@santafe-conicet.gov.ar (P. Aguirre), mussati@santafe-conicet.gov.ar (S. Mussati).

0011-9164/$ – see front matter © 2012 Elsevier B.V. All rights reserved.
http://dx.doi.org/10.1016/j.desal.2012.10.033

carry out comprehensive parametric studies to determine design and operating conditions that can lead to lower irreversibility and higher process efficiency. The use of parametric simulations for optimization purpose is well suitable for small-size problems when only a few optimization variables are considered.

Yılmaz and Söylemez [3] developed a mathematical model of a Multi-Effect Evaporation Forward-Feed (MEE-FF) seawater desalination system using hybrid renewable energy sources (solar flat-plate collector and wind turbine) in Turkey. The system model includes the basic thermodynamic laws, continuity equation, heat transfer equations and the thermodynamic relations which are applied to each sub-system. A simulation program was built with Visual Basic programming language. Hourly values of solar radiation flux on horizontal surface, ambient temperatures, wind velocities and seawater temperatures have been measured for ten years (1999 to 2009) and they have been used in 18 stations to obtain more reliable and realistic simulation results. Simulation results of the developed mathematical model were compared with the literature with satisfactory results making feasible to compare the stations from the point of view of renewable energy potential.

Sayyaadi and Saffari [4] carried out a thermoeconomic optimization of a multi effect distillation (MED) desalination system with thermo-vapor compressor (TVC). The authors presented a complete expression of the product and fuel in the exergy analysis of the MED–TVC system. The economics model of the system was developed based on the Total Revenue Requirement method (TRR method). The optimization problem involved six decision variables and the appropriate feasibility and engineering constraints. The optimization process was carried out using genetic algorithm. Improvements were obtained in all costing elements of the optimized system. The results showed that the thermoeconomic optimization aims at reduction of subcomponent costs by either reducing the cost of inefficiencies, of investment or the operating cost, considered being the most dominant cost-items.

Khademi et al. [6] presented the steady-state simulation and optimization of a six-effect evaporator and the provision of its relevant software package. In this investigation, the modeling equations of each of the existing building blocks are written in steady-state conditions. These equations have been used for simulation and process optimization of the entire vaporizing unit because of the simplifying assumptions. The effects of different parameters on the steam consumption, on the distilled water production and on the GOR are presented. The feed-mass flow rate, the condenser pressure and operating time were optimized for this system. The simulation results are in good agreement with design data.

Abdel-Jabbar et al. [7] developed a computer package based on visual basic code to simulate both single and multiple effect evaporation desalination systems (SEE and MEE). The package features design calculations of heat transfer area, power consumption, and costing. The package is user-friendly and is equipped with interactive menus for report and form printing, file saving and retrieving, help files, and tutorial. Model predictions generated from the code are validated against actual field data and they showed a very good agreement.

Darwish et al. [8] and Ali and El-Fiqi [14] analyzed different multistage and multi-effect desalination systems. The influence of the main process parameters of fresh water production on the unit cost was investigated via simulation. The parameters included were plant performance ratio (PR), specific flow rate of brine, top brine temperature, and specific total heat transfer area. Aybar [11] considered a multi-effect desalination system using waste heat of a power plant as energy source. A simple thermodynamic analysis of the system was performed by using energy and mass balance equations.

El-Dessouky et al. [15] compared different configurations for MEE systems: parallel and parallel/cross flow arrangements. The results showed that the parallel/cross feed MEE system has the best performance. However, the parallel flow system has similar performance characteristics. Moreover, its design, construction, and operation are simpler. The authors also presented the effect of the heating steam temperature and the seawater salinity on the performance ratio, the specific total heat transfer area, the specific cooling water flow rate, and the conversion ratio. They concluded that both, the specific total heat transfer area and the performance ratio decrease with increasing heating steam temperature and, therefore, the process should be optimized among these parameters.

Different mathematical models were also developed and used to optimize operating conditions via simulation (parametric optimization), that is, the models were solved several times using different values of one or more operating variables and then the optimal values were determined by inspection of the objective function values.

Kamali et al. [9] and Kamali and Mohebbinia [10] summarized a parametric optimization technique for the tube size and arrangement of tube bundle inside the MED-TVC system (Multi Effect Desalination with Thermal Vapor Compression) in order to increase the process performance. For this purpose, the authors developed a simulation model of MED-TVC system and the influence of all factors on total capacity, performance ratio, temperature difference between effects and pressure on each effect to select the optimum size and arrangement of tubes was investigated. The simulation package was applied for a specified capacity in order to achieve the best size and arrangement for tube bundles of the system. Authors conclude that the system designed according to results of the simulation package, had a higher performance in comparison with two current systems. The comparison between the simulation results and experimental data well proves optimization method's validity.

In contrast to the articles mentioned above, this paper deals with the simultaneous optimization of the stream flow-patterns (synthesis), the size of each evaporation effect (sizing) and the operating conditions of the entire MEE unit. A simple and predictive steady-state model was developed via mathematical programming and implemented in an advanced tool (GAMS). The model is based on mass and energy balances including design equations to compute heat transfer areas in preheaters, evaporation effects and condenser. In addition, it was developed in such way that embeds some alternative flow-patterns for distillate and vapor streams which have been simultaneously optimized.

In order to verify and check the accuracy of the proposed mathematical model, the outputs have been compared with operating values taken from a real plant and also with values reported by other authors. For this purpose, the model has been used as a simulator, since many optimization variables have been fixed at known values. Once the model was successfully verified, it was applied for optimization purpose. In this paper, the simulated and optimized results are presented and discussed in detail through different case studies.

The paper is outlined as follows. Section 2 briefly describes the MEE process. Section 3 presents the problem formulation. Section 4 summarizes the assumptions and describes the mathematical model. Section 5 discusses the simulated and optimized results obtained from the model. Finally, Section 6 summarizes the conclusions of the paper.

2. Process description

Fig. 1 shows a conventional MEE forward feed scheme. As it can be seen, it consists of several evaporation effects in which fresh water is obtained as a consequence of the evaporation of seawater. Depending on the feed flow-pattern (seawater), the MEE process can be operated according to different arrangements (forward feed, parallel feed, mixed feed and backward feed). In the forward feed scheme, both brine and heating vapor streams flow in the same direction; hence the first effect operates at the lowest salinity and at the highest temperature.

Fig. 2 illustrates a schematic representation of the “jth” evaporation effect. Each one of the effects is composed by a preheater, an evaporation effect and a distillate flash chamber.

As shown in Fig. 1, the feed stream (F^{feed}) passes through the condenser where it exchanges heat with vapors formed in the last effect

($V^b_n + V^{fb}_n + V^{fd}_n$) and increases its temperature from TF^{feed} to TF^c. After that, a part of this stream F^c, hereafter named as cooling water, is rejected to the sea and the remaining feed (F) is heated successively from TF^c to TF^p_1as it flows through the preheaters. Steam is supplied to the first effect as heating medium to heat the seawater stream (F) from TF^p_1 to the boiling temperature TV^b_1, after that it is sprayed over the outside surface of the evaporator tubes and part of it evaporates and produces an amount of vapor (V^b_1). Then, part of $V^b_1$is used in the first preheater to increase the seawater temperature from TF^p_2 to TF^p_1, and the remaining vapor flows as heating vapor to the second effect. The non-evaporated seawater from the first effect (B_1) enters the second effect as feed. From the second effect onward, fresh water is produced inside the effect by two different mechanisms, evaporation (V^b_j) and flashing (V^{fb}_j). After that, the resulting vapors condense and the distillate ($D^e_j + D^p_{j-1}$) goes to a flashing box where a pressure reduction make it flash, generating another vapor stream (V^{fb}_j). Both flashing streams are used to heat the feed stream. The vapor stream generated by evaporation is supplied to the next effect to be used as heating vapor and the non-evaporated seawater (B_j) enters the next effect as feed. Then, the processes of evaporation, condensation, flashing and heating explained above are sequentially repeated until the last effect. As it can be clearly seen in Figs. 1 and 2, the total heat transfer area of the MEE system is given by N evaporators, N-1 preheaters and a down-condenser. The heat transfer area in the first effect can be separated in two terms: A^b_1 which is used for seawater heating and A^e_1 which is used for seawater evaporation. It should be noted that A^b_2 to A^b_N are not included in the model because in these effects there is no seawater heating. In contrast to this, seawater evaporation is performed from j = 2 to j = N, and therefore, A^e_2 to A^e_N were considered in the model. The investment and operating costs are mainly given by the total heat transfer area and the steam used in the first effect as heating medium.

The following are the main process parameters widely used to analyze the global performance of MEE systems:

a) Performance Ratio (PR) is the relationship between the amount of distillate produced and the steam supplied as heating medium,
b) Specific total heat transfer area (sA), defined as the ratio between the total heat transfer area and the amount of distillate produced,
c) Conversion Ratio (CR), defined as the ratio between the amount of distillate produced and the feed seawater flow-rate,
d) Specific cooling water rate (sWc) defined as the ratio between cooling water flow-rate and the amount of distillate produced,
e) Specific total heat (sQ), defined as the ratio between the total heat and the total amount of distillate produced.

As can be easily concluded, there exist several trade-offs between the process variables which strongly depend on the design specifications and the objective function used. As will be explained later, the optimization problem studied in this paper consists on determining the best flow-patterns for distillate and vapor streams, the equipment sizing and the operating conditions for a given heating utility consumption and fresh water demand. Thus, the only free variable that can be optimized to increase the process efficiency is the total heat transfer area. That is why the selected objective function was the total specific heat transfer area (minimization).

3. Problem statement

This paper deals with the development of a mathematical model for the simultaneous optimization of the synthesis, the sizing and the operating conditions of the MEE process considering the flow-patterns for the distillate and vapor as optimization variables. Thus, the mathematical model was developed in such a way to embed several alternative configurations including the conventional ones.

First, the proposed model was used to optimize the conventional configuration shown in Figs. 1 and 2 (Section 5.1). This optimization problem (hereafter named as OP1) assumes that the flow-patterns for all streams are known and the total heat consumed is given (fixed). The proposed objective function for minimization was the specific total heat transfer area (sA) satisfying a specific fresh water demand. Then, the proposed model was used to solve a second optimization problem (hereafter named as OP2), in which, in contrast to OP1, the flow-patterns are considered as optimization variables as Fig. 3 clearly shows (Section 5.2). The objective function is kept equal to the previous case (minimize sA) and the total heat consumed and the distilled water production were fixed.

Table 1 summarizes both optimization problems, OP1 and OP2.

In order to develop a complete mathematical model to solve problems P1 and P2, the configuration shown in Fig. 2 is properly extended as Fig. 3 illustrates. Thus, the resulting model embeds several flow-patterns for some streams (alternative and conventional arrangements).

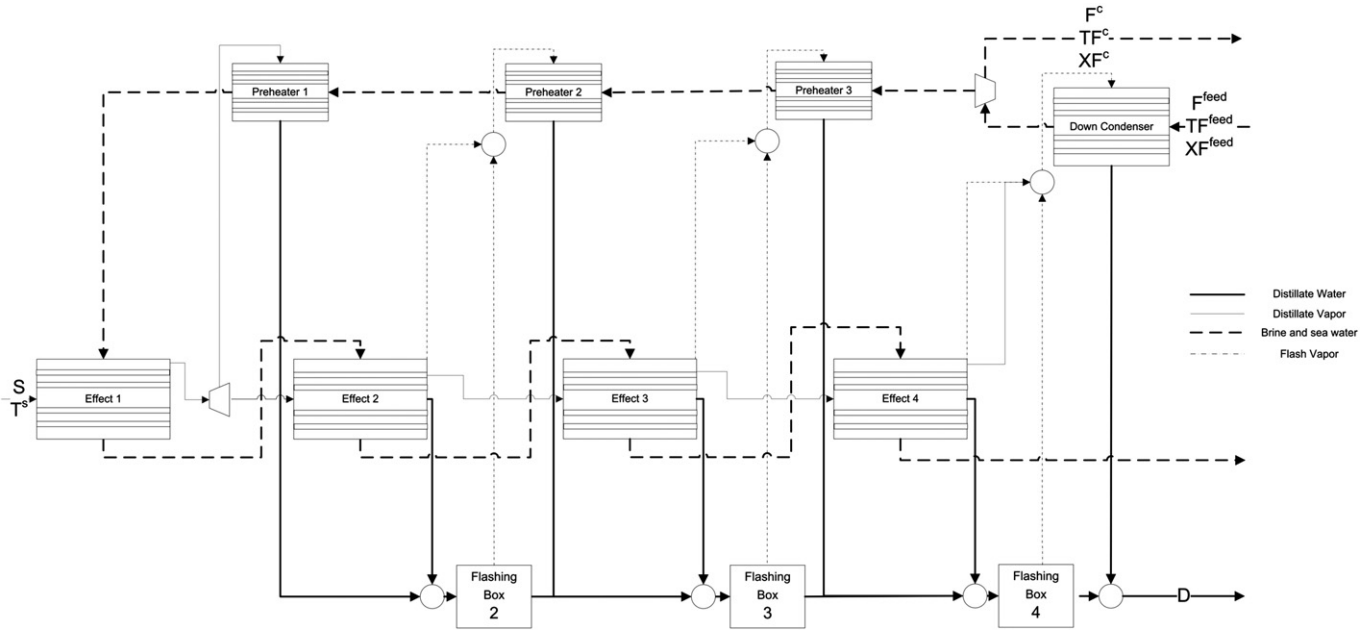

Fig. 1. Conventional of a Multi-Effect Evaporation (MEE) process (forward feed configuration).

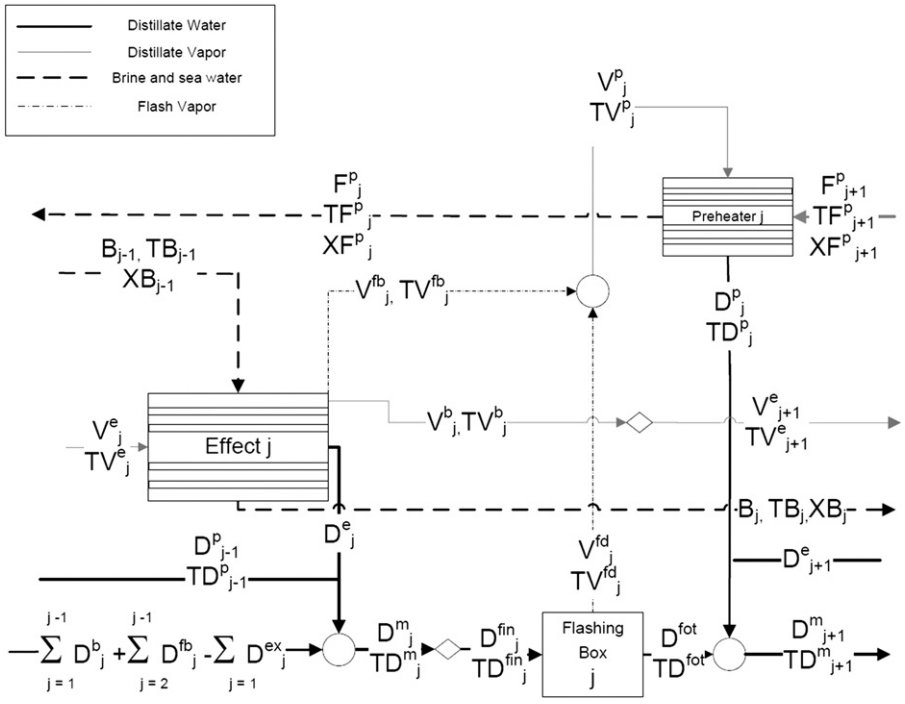

Fig. 2. A schematic representation of the "jth" evaporation effect for the forward feed configuration.

Precisely, beside the conventional stream flow-patterns, the following alternatives for vapor and distillate streams are also embedded:

- Part of the vapor (V^{b}_{j}) produced by seawater evaporation can also be used, together with the vapor formed by flashing (both from brine (V^{fb}_{j}) and from distillate (V^{fd}_{j})), to increase the seawater temperature (TF^{P}_{j+1}). Thus, the total amount of vapor that can be used in the preheater $(j+1)$ as heating medium is given by $(V^{b}_{j}+V^{fb}_{j}+V^{fd}_{j}-V^{e}_{j+1})$, while in the conventional configuration V^{b}_{j} is used only for brine evaporation in the next effect $(j+1)$. In

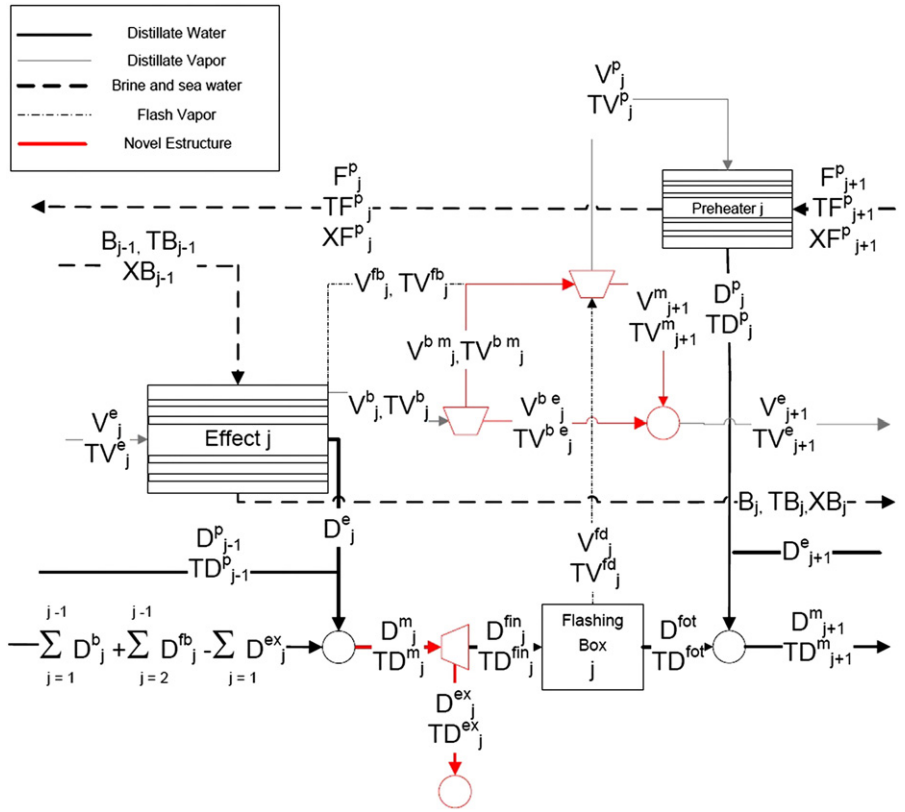

Fig. 3. A schematic representation of the "jth" evaporation effect for the novel configuration.

addition, the model also includes (sea Fig. 3) the option of using part of V^{fb}_j or V^{fd}_j or eventually both ($V^{fb}_j + V^{fd}_j$) as heating medium for brine evaporation in the next effect (j + 1).
- Distillate extraction in each effect (D^{ex}_j).

In the next section, the complete mathematical model, including the assumptions made, is presented in detail.

4. Assumptions and mathematical model

4.1. Assumptions

The following are the main assumptions used to derive the mathematical model.

- Boiling Point Elevation (BPE) is considered as a constant and a known value is assumed.
- The non-equilibrium allowance (NEA) is neglected.
- Pressure drop in the demister and during the vapor condensation process is neglected.
- A constant and known value is assumed for each one of the specific heat capacities of each one of the streams.
- The effect of fouling factors and the presence of non-condensable gasses on the heat transfer coefficients in the evaporators, preheaters and the condenser are neglected.
- The temperature drop, the distillate production and the heat transfer areas in each one of the effects may be different. In other words,no equality constraints are imposed in the model for these variables.

4.2. Mathematical model

Basically, the steady-state mathematical model of the MEE forward feed schema, including the different stream configurations shown in Fig. 3, is based on mass and energy balances around each one of the process-units (mixers, splitters, evaporation effects, distillate flashing chambers and preheaters). Precisely, the resulting model involves the following constraints.

4.2.1. Mass balance

First effect:

$$F^p_j = V^b_j + B_j \quad j = 1 \tag{1}$$

$$F^p_j XF^p_j = V^b_j XV^b_j + B_j XB_j \quad j = 1 \tag{2}$$

$$V^{bm}_j = V^p_j + V^m_{j+1} \quad j = 1 \tag{3}$$

$$V^{be}_j + V^m_{j+1} = V^e_{j+1} \quad j = 1 \tag{4}$$

$$D^e_{j+1} + D^p_j = D^m_{j+1} \quad j = 1\,. \tag{5}$$

Table 1
Optimization problems.

Optimization problem OP1	Optimization problem OP2
Min (sA)	Min (sA)
Subject to:	Subject to:
–) Mass and energy balances	–) Mass and energy balances
–) Design equations	–) Design equations
–) Conventional flow-patterns for distillate and vapor streams	–) Alternative flow-patterns for distillate and vapor streams
–) Heat entering the first effect $\le Q_0$[a]	–) Heat entering the first effect $\le Q_0$[a]

[a] Where Q_0 is a model parameter (known and fixed value).

Last effect:

$$F^p_j + F^c = F^{feed} \quad j = N \tag{6}$$

$$XF^p_j = XF^{feed} \quad j = N \tag{7}$$

$$XF^c = XF^{feed} \tag{8}$$

$$V^{fb}_j + V^{bm}_j + V^{fd}_j = V^p_j \quad j = N \tag{9}$$

$$D^{fot}_j + D^{ext} + D^p_j = D \quad j = N\,. \tag{10}$$

The other jth effects:

$$V^b_j + V^{fb}_j + B_j = B_{j-1} \quad \forall j > 1 \tag{11}$$

$$B_j XB_j = B_{j-1} XB_{j-1} \quad \forall j > 1 \tag{12}$$

$$V^m_j + V^p_{j-1} = V^{fb}_{j-1} + V^{bm}_{j-1} + V^{fd}_{j-1} \quad \forall j > 2 \tag{13}$$

$$V^e_j = V^{be}_{j-1} + V^m_j \quad \forall j > 2 \tag{14}$$

$$F^p_j = F^p_{j+1} \quad \forall j \neq N \tag{15}$$

$$XF^p_j = XF^p_{j-1} \quad \forall j \neq N \tag{16}$$

$$D^m_j = D^e_j + D^p_{j-1} + D^{fot}_{j-1} \quad \forall j > 2 \tag{17}$$

$$D^{fin}_j = D^{fot}_j + D^{fd}_j \quad \forall j > 1 \tag{18}$$

$$D^{ex}_j + D^{fin}_j = D^m_j \quad \forall j > 1\,. \tag{19}$$

For all effects:

$$V^b_j = V^{bm}_j + V^{be}_j \quad \forall j\,. \tag{20}$$

4.2.2. Energy balance

First effect:

$$Q = S\lambda^s = V^b_j \lambda_j + F^p_j Cp\left(TB_j - TF^p_j\right) \quad j = 1 \tag{21}$$

$$TV^{bm}_j = TV^p_j \quad j = 1 \tag{22}$$

$$TV^{bm}_j = TV^m_{j+1} \quad j = 1 \tag{23}$$

$$V^{be}_j HV^{be}_j + V^m_{j+1} HV^m_{j+1} = V^e_{j+1} HV^e_{j+1} \quad j = 1 \tag{24}$$

$$D^e_{j+1} HD^e_{j+1} + D^p_j HD^p_j = D^m_{j+1} HD^m_{j+1} \quad j = 1\,. \tag{25}$$

Last effect:

$$TF^p_j = TF^{feed} \quad j = N \tag{26}$$

$$TF^c = TF^{feed} \tag{27}$$

$$V^{fb}_j HV^{fb}_j + V^{bm}_j HV^{bm}_j + V^{fd}_j HV^{fd}_j = V^p_j HV^p_j \quad j = N \tag{28}$$

$$D^{fot}_j HD^{fot}_j + D^{ext} HD^{ext} + D^p_j HD^p_j = DHD \quad j = N \tag{29}$$

$$V^p_j \lambda_j = F^{feed} Cp\left(TF^p_j - TF^{feed}\right) \quad j = N\,. \tag{30}$$

The other jth effects:

$$V^{b}{}_{j}\lambda_{j} = V^{e}{}_{j}\lambda_{j-1} \quad \forall j > 1 \tag{31}$$

$$V^{fb}{}_{j}\lambda_{j}{}^{fb} = B_{j-1}Cp\left(TB_{j-1} - TV_{j}^{fb}\right) \quad \forall j > 1 \tag{32}$$

$$TV_{j}^{fb} = TB_{j} \quad \forall j > 1 \tag{33}$$

$$V^{p}{}_{j}\lambda_{j} = F_{j}Cp\left(TF^{p}{}_{j} - TF^{p}{}_{j+1}\right) \quad \forall j \neq N \tag{34}$$

$$D^{fd}{}_{j}\lambda_{j}{}^{fd} = D^{fin}{}_{j}Cp\left(TD^{fin}{}_{j} - TD_{j}^{fd}\right) \quad \forall j > 1 \tag{35}$$

$$D^{m}{}_{j}HD_{j}^{m} = D^{fot}{}_{j-1}HD_{j-1}^{fot} + D^{b}{}_{j}HD^{b}{}_{j} + D^{p}{}_{j-1}HD_{j-1}^{p} \quad \forall j > 1 \tag{36}$$

$$TV_{j}^{fd} = TB_{j} - BPE \quad \forall j > 1 \tag{37}$$

$$TD^{m}{}_{j} = TD^{fin}{}_{j} \quad \forall j > 1 \tag{38}$$

$$TD^{m}{}_{j} = TD^{ex}{}_{j} \quad \forall j > 1 \tag{39}$$

$$V^{p}{}_{j-1}HV^{p}{}_{j-1} + V^{m}{}_{j}HV^{m}{}_{j} = V^{fb}{}_{j-1}HV^{fb}{}_{j-1} + V^{bm}{}_{j-1}HV^{bm}{}_{j-1} + V^{fd}{}_{j-1}HV^{fd}{}_{j-1} \forall j > 2 \tag{40}$$

$$V^{e}{}_{j}HV^{e}{}_{j} = V^{be}{}_{j-1}HV^{be}{}_{j-1} + V^{m}{}_{j}HV^{m}{}_{j} \quad \forall j > 2 \tag{41}$$

$$TF^{p}{}_{j} = TF^{p}{}_{j+1} \quad \forall j \neq N \tag{42}$$

$$D^{m}{}_{j}HD^{m}{}_{j} = D^{e}{}_{j}TD^{e}{}_{j} + D^{p}{}_{j-1}HD^{p}{}_{j-1} + D^{fot}{}_{j-1}HD^{fot}{}_{j-1} \quad \forall j > 2 \tag{43}$$

$$TD^{ex}{}_{j} = D^{m}{}_{j} \quad \forall j > 1 \tag{44}$$

$$TD^{fin}{}_{j} = D^{m}{}_{j} \quad \forall j > 1\,. \tag{45}$$

For all effects:

$$TV^{b}{}_{j} = TV^{bm}{}_{j} \quad \forall j \tag{46}$$

$$TV^{b}{}_{j} = TV^{be}{}_{j} \quad \forall j \tag{47}$$

$$TV^{b}{}_{j} = TB_{j} - BPE \quad \forall j \tag{48}$$

$$TD^{p}{}_{j} = TB_{j} - BPE \quad \forall j\,. \tag{49}$$

4.2.3. Heat transfer areas

First effect:

$$F^{p}{}_{j}Cp\left(TB_{j} - TF^{p}{}_{j}\right) = A^{b}{}_{j}U^{b}LMTD_{j} \quad j = 1 \tag{50}$$

$$V^{b}{}_{j}\lambda_{j} = A_{j}{}^{e}U^{e}\left(T^{s} - TB_{j}\right) \quad j = 1 \tag{51}$$

$$LMTD_{j} = \frac{\left(TB_{j} - TF^{p}{}_{j}\right)}{\ln\left(\frac{T^{s} - TF^{p}{}_{j}}{T^{s} - TB_{j}}\right)} \quad j = 1\,. \tag{52}$$

The other jth effects:

$$V^{b}{}_{j}\lambda_{j} = A_{j}{}^{e}U^{e}\left(TV_{j}{}^{b} - TB_{j}\right) \quad \forall j > 1 \tag{53}$$

$$V^{p}{}_{j}\lambda_{j} = A_{j}{}^{p}U^{p}LMTD_{j}{}^{p} \quad \forall j \neq N \tag{54}$$

$$LMTD^{p}{}_{j} = \frac{\left(TF^{p}{}_{j} - TF^{p}{}_{j+1}\right)}{\ln\left(\frac{TD^{p}{}_{j} - TF^{p}{}_{j+1}}{TD^{p}{}_{j} - TF^{p}{}_{j}}\right)} \quad \forall j \neq N\,. \tag{55}$$

Last effect:

$$V^{p}{}_{j}\lambda_{j} = A^{c}U^{c}LMTD^{c} \quad j = N \tag{56}$$

$$LMTD^{c} = \frac{\left(TF^{p}{}_{j} - TF^{feed}\right)}{\ln\left(\frac{TD^{p}{}_{j} - TF^{feed}}{TD^{p}{}_{j} - TF^{p}{}_{j}}\right)} \quad j = N\,. \tag{57}$$

4.2.4. Inequality constrains

To avoid temperature crosses among stages, following conditions must be satisfy:

$$T_{j} > T_{j+1} \quad \forall j \neq N \tag{58}$$

$$T^{f}{}_{j} > T^{f}{}_{j+1} \quad \forall j \neq N \tag{59}$$

$$F = F^{p}{}_{j} \quad j = N \tag{60}$$

$$B = B_{j} \quad j = N\,. \tag{61}$$

Correlations

$$H_{j} = -0.033635409 + 4.207557011\ T_{j} - 6.200339 \times 10^{-4}\,T_{j}{}^{2} + 4.459374 \times 10^{-6}T_{j}{}^{3} \forall j > 1. \tag{62}$$

To measure the system efficiency:

$$PR = \frac{D}{S} \tag{63}$$

$$CR = \frac{D}{F} \tag{64}$$

$$sCW = \frac{W_{C}}{D} \tag{65}$$

$$sA = \frac{A}{D} \tag{66}$$

$$A = \sum_{i=1}^{N}\left(A_{j}^{e} + A_{j}^{p}\right) + A_{1}^{b}. \tag{67}$$

Other constraints:

$$D^{ext} = \sum_{j=2}^{N} D^{ex}{}_{j} \tag{68}$$

$$\Delta T_{j} = TV_{j}{}^{b} - TB_{j} \quad \forall j > 1\,. \tag{69}$$

The following constraints are imposed to guarantee a uniform heat transfer area distribution (UHTA) in preheaters and evaporation effects. These constraints should be removed for non-uniform heat transfer area distributions (NUHTA).

$$A^{p}{}_{j} = A^{p}{}_{j+1} \quad \forall j > N-1 \tag{70}$$

$$A^{e}{}_{j} = A^{e}{}_{j-1} \quad \forall j > 2\,. \tag{71}$$

The following constraint guarantees an equal temperature drop along the effects:

$$\Delta T_j = \Delta T_{j-1} \quad \forall j > 2 . \tag{72}$$

4.3. Implementation aspect

The optimization model involves 469 constraints (equalities and inequalities). The total number of variables is 375. It should be noticed that global optimal solution cannot be guaranteed due to the presence of non-convex constraints.

As mentioned earlier the resulting steady-state model is non linear (NLP) and was implemented in an advanced tool, GAMS. The used tool is a high-level modeling system for mathematical programming and optimization. It deals with algebraic equations which are solved simultaneously. GAMS is widely used for many areas and applications and includes a large number of solvers for mathematical programming models: linear programming (LP), mixed integer programming (MIP), non linear programming (NLP) and mixed integer non linear programming (MINLP) problems. GAMS includes several NLP local solvers: CONOPT, SNOPT and MINOS5 algorithms. They are all based on fairly different mathematical algorithms. A more detailed explanation of how the NLP solvers work can be found in Brooke et al. [16]. CONOPT is a feasible path solver based on the Generalized Reduced Gradient (GRG) and it has been designed for large and sparse models (large number of variables and equations) and from our experience, the proposed model could be efficiently solved by using CONOPT. Certainly, this was the solver used in this case and in all cases the model was successfully solved at low computational cost, that is, the convergence was reached in a few iterations and a short CPU time.

An Intel Core i7 2230 M 2.20 GHz processor with 8 GB RAM has been used to perform the simulations and optimizations.

5. Discussion of results

In this section, two case studies are presented in order to discuss simulated and optimized results. The first case study deals with the verification of the proposed model (simulation) and the second case study discusses and compares the optimization of the conventional and novel stream flow-patterns. Thus, the mathematical model presented above (Eqs. (1) to (72)) is used to solve different case studies for either the conventional configuration or the most complete model which embeds different alternatives of the flow-patterns for distillate and vapor streams.

5.1. Case study 1 (OP1-simulation)

5.1.1. Model verification

In order to verify the accuracy of the proposed model, the predicted results have been compared to those reported by Darwish et al. [8] and El-Dessousky and Ettouney [17]. Only for a valid comparison, the conventional configuration was considered and the proposed model was used here as a "simulator", that is, the mathematical model was solved with zero degrees of freedom taking as objective function the specific total heat transfer area. For this reason, the values of some optimization variables related to the novel flow-patterns, were set to zero (D^{ext}, $V^{bm}{}_i$, $V^{m}{}_i$) and others were set to fixed values (D, TF^{feed}, T^c, TB_1, XF^{feed}, XB_6, S, Q), in accordance with the literature [8,17].

In addition, Eqs. (70) and (71) were included in order to assure uniform heat transfer area distributions (UHTA) along the effects and preheaters. Eq. (72) was also considered to assure equal temperature differences along the evaporation effects.

Table 2 lists the numerical values of variables and parameters used for comparison.

Tables 3 and 4 compare the numerical values obtained by the model to those values reported by Darwish et al. For a more reliable and precise reproducibility of the results and model verification, results are presented with a different number of significant digits of precision.

From Table 3, it is possible to observe that the predicted values for the inlet seawater flow-rate (F^{feed}) and the heat transfer area in the down condenser (A_c) are slightly greater than those reported by Darwish et al. (4.72%). The observed differences may be explained on the basis of the assumptions used to derive the current model, which are different to those considered by Darwish et al. In fact, the process configuration considered in this paper uses the entire vapor formed in the last effect ($V^{b}{}_n + V^{fb}{}_n + V^{fd}{}_n$) to heat the incoming seawater, in contrast to the configuration considered in Darwish et al., where the distillate formed in the last flashing box in not used for heating purpose ($V^{fd}{}_n$).

Another difference between the predicted and reported values that can be observed in Table 3 is in the prediction of the heat transfer area in the first evaporation effect ($A^e{}_1$). Certainly, the value reported by Darwish et al. is 15.56% higher than the value predicted by the current model. This difference is a consequence of the simplifying assumptions considered by Darwish to compute the heat transfer area of the first effect assuming that the total energy provided by the heating-utility stream or total heat consumed (Q) is only used for brine evaporation and not for brine heating. Therefore, Darwish et al. did not consider the heat transfer area for seawater heating and it was computed as follows: $S\lambda^s = A_1 U^e (TB_1 - BPE - TB_2)$. On the contrary, the current model, the heat transfer is used both for brine evaporation and for brine heating (Eqs. (50) and (51)), thus, a more realistic value is obtained for the heat transfer area.

Table 4 lists the values simulated for each one of the variables which are all in good agreement with those reported by Darwish et al.

The output results obtained by the developed model were also compared with data reported by El-Dessouky and Ettouney [17] which are widely used by other authors for comparison purpose. It should be mentioned, however, that the model derived by El-Dessouky and Ettouney is a bit more complete than the model presented in this paper. In fact, it includes: pressure drops, geometric design (dimensions: length, height and width) and correlations to compute heat transfer coefficients. Then, the idea behind the comparison is to assess the accuracy of the proposed simplified model with a detailed mathematical model. Table 5 summarizes the basic assumptions involved in both models.

The comparison has been performed in terms of the specific total heat transfer area, the number of effects and the top brine temperature, using the parameter values shown in Table 6.

The values of the specific total heat transfer areas predicted by the proposed model and those reported by El-Dessouky for six evaporation effects, varying the steam temperatures (heating utility) and the overall heat transfer coefficients, are illustrated in Fig. 4. As it is clearly shown, there is a good accuracy between the results predicted by the simplified model and the detailed model developed by El-Dessouky for $U = 2.10$ kW/(m^2 °C). Fig. 5 illustrates the variation of the specific

Table 2
Numerical values assumed for model verification (Darwish et al. [8]).

Parameter	Unit	Value
Cp	(kJ/kg °C)	4.00
D	(kg/s)	393.94
BPE	(°C)	1.00
λ	(kJ/kg)	2333.00
TF^{feed}	(°C)	26.00
T^c	(°C)	35.00
XF^{feed}	(ppm)	45,978.90
XB_6	(ppm)	72,000.00
S	(kg/s)	72.80
Q	(kJ/s)	169,842.40
T^s	(°C)	70.00
TB_1	(°C)	65.00
$U^e = U^p = U^c$	(kW\m^2 °C)	3.00
N		6

Table 3
Comparison between predicted and published values.

Parameters		This work	Darwish et al. 8
F	(kg/s)	1090.03	1090.00
PR	(kg/s of D/(kg/s of S))	5.40	5.40
sWc	(kg/s of F^c/(kg/s of D))	8.29	7.78
CR	(kg/s of D/(kg/s of F))	0.36	0.36
sA	(m^2/(kg/s of D))	180.50	184.89
F^{feed}	(kg/s)	4354.40	4157.00
F^c	(kg/s)	3264.36	3067.00
A^c	(m^2)	9897.22	9448.85
$A^e{}_1$	(m^2)	11,133.87	12,866.84
A	(m^2)	80,999.58	82,282.30

heat transfer area with the number of effects and heating steam temperature for U = 2.1 kW/(m^2 °C). Therefore, it is possible to conclude that simplified models can be effectively used to predict the behavior of the main process parameters. In addition, they can be also efficiently used in a sequential solution strategy; solutions obtained from simplified models are good initial values for solving another, more detailed model, improving its convergence.

It is also possible to observe in Figs. 4 and 5 that the specific heat transfer area increases as the number of effects increases and the overall heat transfer coefficient and the heating-steam temperature decreases. This occurs because increasing the number of effects and decreasing the heating steam temperature decreases the temperature drop per effect, and decreasing the overall heat transfer coefficient decrease the heat transmission and the system efficiency as well.

5.1.2. Sensitivity analysis

In order to investigate the influence of each one of the model parameters (P_j) on the objective function (OF) a parameter sensitivity analysis was performed for case study 1. The aim of the sensitivity analysis is to estimate the rate of change in the model outputs with respect to changes in the model inputs. Such knowledge is important for (a) evaluating the applicability of the model, (b) determining parameters for which it is important to have more accurate values, and (c) understanding the behavior of the system being modeled. The choice of a sensitivity analysis method depends mainly on (a) the sensitivity measure employed, (b) the desired accuracy in the estimates of the sensitivity measure, and (c) the computational cost involved.

In this paper, the analysis is performed based on a local sensitivity method that computes the local gradients of the objective function, the total heat transfer area, in regard to infinitesimal parameter variations. Specifically, the analysis is focused on the relative marginal values for each one of the model parameters (RMV_j) which is defined as follows:

$$RMV_j = \frac{\frac{\partial(OF)}{OF}}{\frac{\partial(P_j)}{P_j}} = \frac{P_j}{OF}\ PMC_j \quad \forall j \tag{73}$$

Table 5
Comparison of assumptions assumed in El-Desouky and in this work.

Parameters	El-Dessouky and Ettouney [17]	This work
Heat transfer area [a]	Constant	Constant
BPE	Variable	Constant
NEA	Variable	Constant
Non condensable gasses	Yes	No
Pressure drop	Yes	No
Geometrical model	Yes	No
Vapor salt free	Yes	Yes
Energy loss to the ambient	No	No
λ	Variable	Constant
Cp	Variable	Constant
$U^e = U^p = U^c$	Variable	Constant
Number of feed preheaters	N − 2	N − 1

[a] Heat transfer area for evaporators and preheaters.

where PMC_j refers to the parameter marginal cost and is computed as: $\frac{\partial(OF)}{\partial(P_j)}$.

The direction of the change on the objective function is given by the sign of the RMV. As it is here defined, a positive relative marginal implies an increase in the total heat transfer area when increasing the parameter value in 1%. Table 7 reports the values of RMV obtained for each one of the parameters and they are arranged according to their effect on the specific total heat transfer area. It is important to notice that these parameters correspond to different categories: design, physicochemical and operatives, and all this categories have their influence in the objective function.

It can be observed that the total heat transfer area is strongly influenced by Ts, S, $U^e{}_i$,$U^p{}_i$,$U^c{}_i$,TB_6, λ and D. In particular, the total heat transfer area decreases in 2.0% (from 80999.58 to 79379.58) when T_s or S is increased in 1.0%. In the same way, the total heat transfer area decreases in 1.0% if the values of the global heat transfer coefficients are increased in 1.0%. On the other hand, the total heat transfer area increases in 3.0% when the distillate production increases in 1.0% and it increases in almost 0.77% for TB_6 or λ. The remaining model parameters such as XF^{feed}, Cp, BPE, TF^{feed}, TB_1, XB^{up} do not affect significantly the total heat transfer area.

A brief discussion about the effect of TF^{feed} on the total heat transfer area should be introduced. A priori, it might be expected that the total heat transfer area should decrease as TF^{feed} increases. However, the opposite was observed, mainly because the heat transfer area of the down condenser increases as TF^{feed} increases, this occurs because the capacity of the down condenser to condense the vapor produced in the last effect decreased as it is briefly explained below. The distillate demand (D) and the seawater salinity (XF^{feed}) are fixed and have known values, and a maximum allowed salinity for the rejected brine (XB^{up}) was imposed by an upper bond and this maximum value was always reached. In addition, the brine outlet temperature in the last effect (TB_6) and consequently the distillate temperature ($TD^P{}_6$) are also fixed. According to the input data and the mass and energy balances, $D^P{}_6$, $TF^P{}_i$ and T^c are fixed. Then, according to the following constraints, the temperature

Table 4
Simulated values.

Effect	TB	TF^p	V^b	V^{fb}	D	V^{fd}	B	XB	A^e	A^p	ΔT
	(°C)		(kg/s)					(ppm)	(m^2)		
1	65.00	62.00	67.20	0.00	67.20	0.00	1022.83	48,999.39	11,133.87		5.00
2	59.60	56.60	57.10	9.47	66.57	0.62	956.26	52,410.51	10,092.15	1,901.40	4.40
3	54.20	51.20	57.10	8.85	65.95	1.24	890.31	56,293.01	10,092.15	1,901.40	4.40
4	48.80	45.80	57.10	8.24	65.34	1.85	824.96	60,751.96	10,092.15	1,901.40	4.40
5	43.40	40.40	57.10	7.64	64.74	2.45	760.22	65,925.44	10,092.15	1,901.40	4.40
6	38.00	35.00	57.10	7.04	64.14	3.05	696.09	72,000.00	10,092.15	1,901.40	4.40
Total			352.70	41.24	393.94	9.21	5,150.67		61,594.62	9,507.00	27.00

Table 6
Numerical values assumed for model verification (El-Dessouky and Ettouney [17]).

Parameters		
Cp	(kJ/kg °C)	4.00
D	(kg/s)	1.00
BPE	(°C)	1.00
λ	(kJ/kg)	2333.00
TF^{feed}	(°C)	25.00
T^{a}	(°C)	35.00
XF^{feed}	(ppm)	42,000.00
XB_6	(ppm)	70,000.00
$U^e = U^a = U^p$ [a]	(kW/m² °C)	1.80–2.40
T^s [a]	(°C)	60.00–110.00
N [a]		6–12

[a] Parameter varied.

drop ($T^c - TF^{feed}$) decreases as TF^{feed} increases, resulting in a lower value of $LMTD^c$ and therefore in a higher value of A^c.

$$LMTD^c = \frac{\left(TF^p{}_6 - TF^{feed}\right)}{\ln\left(\frac{TD^p{}_6 - TF^{feed}}{TD^p{}_6 - TF^p{}_6}\right)} \tag{74}$$

$$V^p{}_6\lambda_6 = A^c U^c LMTD^c \quad i = 6 \tag{75}$$

5.2. Case study 2 (OP1 and OP2-optimization)

In this section, the optimization problem stated in Section 3 is discussed. The optimal design consists of determining the best flow-patterns for distillate and vapor streams, the equipment sizing and the operating conditions to minimize the total specific heat transfer area for a given heating utility consumption and fresh water demand. The simultaneous optimization of different alternative flow-patterns is performed in order to determine the optimal design of the MEE unit. Optimized results obtained for the novel and the conventional flow-patterns are compared and analyzed.

5.2.1. Optimization of the superstructure embedding alternative flow-patterns

As mentioned earlier, in the proposed configuration, in contrast to the conventional arrangement, the total vapor formed in an effect (vapors formed by the flashing of the brine ($V^{fb}{}_j$) and distillate ($V^{fd}{}_j$) and the vapor formed by the evaporation of the brine ($V^b{}_j$)) can be used in the preheater (j + 1) and/or in the evaporation effect (j + 1). Thus, the amounts of vapor to be derived to the preheater and the evaporation effect will be obtained as a result of the model. In addition, distillate extraction in each one of the distillate plates is also considered as a continuous decision; certainly it may be partially or totally extracted.

In addition, the model is solved separately for the following two assumptions: a) uniform heat transfer area in each preheater and evaporation effect (hereafter named UHTA_OP2 and UHTA_OP1) and b) non-uniform heat transfer area (hereafter named NUHTA_OP2 and NUHTA_OP1).

1. As mentioned earlier in Section 5.1, the mathematical models corresponding to UHTA_OP1 and UHTA_OP2 are given by Eqs. (1) to (71) but for NUHTA_OP1 and NUHTA_OP2 Eqs. (70) and (71) are removed.
2. In addition, in the UHTA_OP2 and UHTA_OP1 models the heat transfer area in all feed preheaters, except the down condenser, is forced to be uniform [Eq. (70)]. This is because the down-condenser has the special function to reject the extra heat of the MEE unit by condensing the entering vapor produced at the last effect which is also used to heat the incoming seawater. Therefore, the heat transfer area required for the down-condenser (A^c) could be different than that required by the remaining preheaters. The outlet temperature at the down-condenser (T^c) could be adjusted by the cooling seawater (F^c). It should also be emphasized that the uniformity of the heat transfer areas related to the evaporation in each effect ($A^e{}_i$) is imposed for all effects, except of the first effect [Eq. (71)].

This is because the first evaporation effect does not only work as an evaporator but also as a preheater and consequently the heat transfer area required for the first effect is greater than that required by the remaining evaporation effects.

Briefly, an optimal distribution of heat transfer area may be obtained when NUHTA_OP1 and NUHTA_OP2 models are solved. In addition, both models include more trade-offs in comparison to the UHTA_OP1 and UHTA_OP2 models. Finally, it should be mentioned that NUHTA_OP2 is the mathematical model that involves the highest freedom degrees because it simultaneously embeds different alternative flow-patterns for distillate and vapor streams and includes the possibility of uniform and non-uniform heat transfer area distributions. Then, models UHTA_OP1 and NUHTA_OP2 can be considered as extreme cases because their freedom degrees.

Table 8 lists the parameter values used for the optimization and Table 9 compares the optimal values obtained for the main variables for each one of the optimization cases.

Table 9 clearly reveals that the minimum total heat transfer area is obtained for NUHTA_OP2, with a total heat transfer area (A) 5.16% lower than that required for UHTA-OP1. The main differences from the novel configuration compared to the conventional one are: the

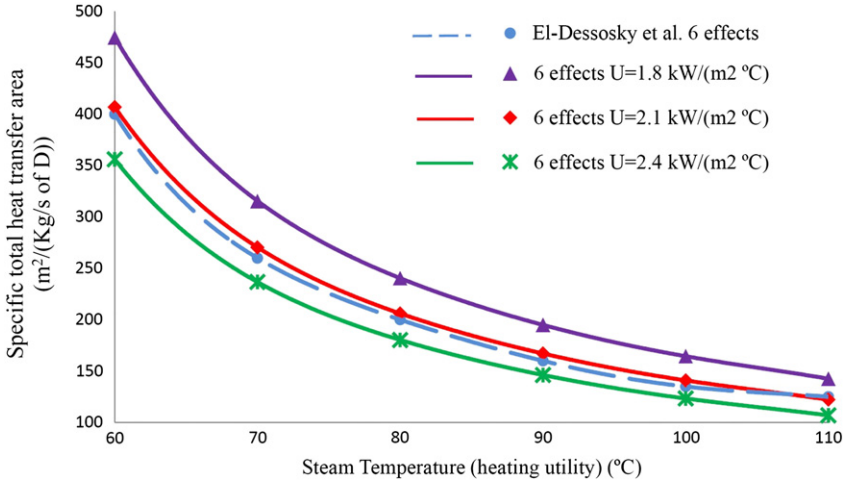

Fig. 4. Specific total heat transfer area vs. heating steam temperature (number of effects = 6).

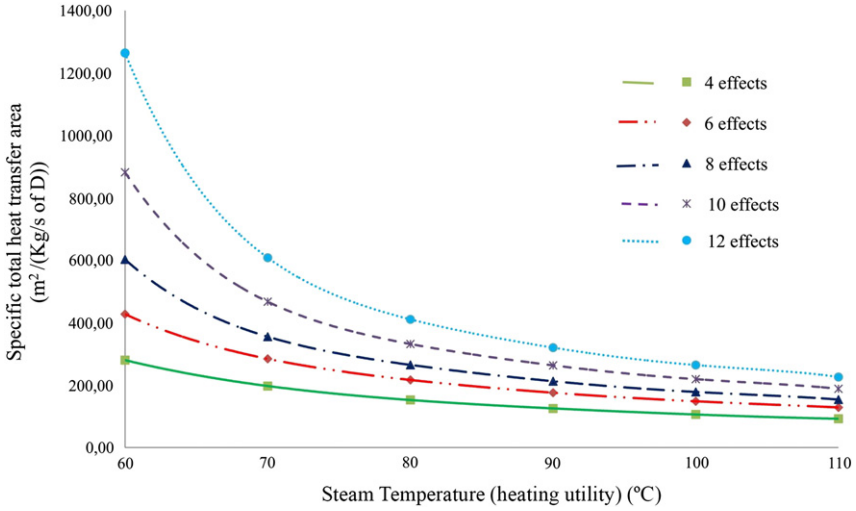

Fig. 5. Specific total heat transfer area and number of effects vs. heating steam temperature (U = 2.10 kW/(m^2 °C)).

opposite trends to allocate heat transfer area in preheaters and down-condenser, being the total heat transfer area in preheaters (A^P) higher than that required by the down-condenser (A^C). It should be mentioned, however, that the seawater temperature leaving the down-condenser (TF^c) reaches the lower bound (26.10 °C), indicating that the down-condenser is only used to condense the vapor formed in the last effect and not to heat the seawater stream. The novel flow-patterns (distillate and vapor) allow allocating the heat transfer area in a different way by varying the condensation temperature (TV^b), the driving forces and the flow-rates, resulting in a decrease of the total heat transfer area. The cooling water (F^c) and the seawater flow-rate stream (F^{feed}) have been significantly increased. However it is important to notice that the increase of mass flow rates (F^{feed} and F^c) will increase not only the power consumption but also the amounts of chemical additives for seawater pretreatment and consequently their corresponding operating costs. For this reason, in order to obtain a final and optimal design, costs (investment and operating costs) should be analyzed. Because in this model the costs are not considered, the fifth column in Table 9 presents the results obtained when an upper bound for F^c is imposed in order to show the influence of F^c on the optimal design. The value for the upper bound used is the optimal value of the UHTA_OP1. Results reveal that the total heat transfer area for NUHTA_OP2, even with the upper bound, is still lower (2.86%) than that required for the conventional configuration.

For the conventional flow patterns, it can also be observed that the total heat transfer area (A) required for UHTA_OP1 is about 2.5% higher than that required for non uniform heat transfer areas (NUHTA_OP1). However, for the novel flow-patters, the total heat transfer area (A) required for UHTA_OP2 is merely a 0.14% higher than that required for non uniform heat transfer areas (NUHTA_OP2).

In order to perform a more detailed comparison, Figs. 6 to 9 illustrate the distribution of temperatures, heat transfer areas and the corresponding driving forces along the MEE unit for both extreme cases (NUHTA_OP2 and UHTA_OP1).

Fig. 6 and 7 reveal that the novel configuration has lower heat transfer area in each evaporation effect and slightly higher heat transfer area in each preheater than the conventional configuration, except by the last effect. The heat transferred from the first evaporation effect to the N-1 evaporator is just a bit lower than from the conventional configuration, but in the last evaporator, the heat transferred is significantly lower than for the conventional configuration. On the other hand, the heat transferred in each preheater is slightly higher for the novel configuration, but the heat transferred in the down condenser is considerably lower than the conventional one.

Figs. 8 and 9 show the optimal temperature and driving force profiles along evaporators and preheaters. Except for the first effect, the driving force profile for brine evaporation decreases smoothly and linearly for the novel configuration, while it is uniform from the conventional configuration. For both models, the driving force in the first effect is about 1 °C higher than in the remaining effects.

Similarly, for the conventional configuration, the driving force profile for preheaters is uniform and it decreases 1 °C in the down condenser. For the novel configuration, instead, the driving force slightly decreases from J = 1 to J = N − 2 and then it increases about 1.0 °C in the last two effects.

Fig. 10 compares the corresponding optimal flow-patterns for both cases. For the novel case (NUHTA_OP2), from j = 2 to j = N − 2,

Table 7
Parameters of the sensitivity analysis.

Parameter	Unit	Value	RMV
D	(kg/s)	393.94	3.05
T^s	(°C)	80.00	−2.17
S	(kg/s)	74.68	−2.11
$U^e = U^p = U^c$	(kW/(m^2 °C))	3.00	−1.00
TB6	(°C)	38.00	0.78
λ	(kJ/kg)	2333.00	0.76
XB^{up}	(ppm)	72,000.00	−0.31
XF^{feed}	(ppm)	45,978.90	0.31
Cp	(kJ/(kg °C))	4.00	0.24
BPE	(°C)	1.00	0.20
TF^{feed}	(°C)	26.00	0.18
TB1	(°C)	65.00	−0.02

Table 8
Parameter values used for optimization.

Parameter	Unit	Value
Cp	(kJ/(kg °C))	4.00
D	(kg/s)	393.94
S	(kg/s)	74.68
BPE	(°C)	1.00
λ	(kJ/kg)	2333.00
T^{feed}	(°C)	26.00
XF^{feed}	(ppm)	45,978.90
XB^{up}	(ppm)	72,000.00
Q	(kJ/s)	174,220.00
sQ	(kJ/s/(kg/s of D))	442.25
$U^e = U^p = U^c$	(kW/(m^2 °C))	3.00
N		6

Table 9
Optimal values for different configurations.

Parameters		Alternative flow-patterns			Conventional flow-patterns	
		NUHTA_OP2	UHTA_OP2	NUHTA_OP2[a]	NUHTA_OP1	UHTA_OP1
T^s	(°C)	80.00	80.00	80.00	80.00	80.00
F^{feed}	(kg/s)	336,113.10	337,558.38	8373.57	29,193.37	8373.57
F^c	(kg/s)	335,023.97	336,468.35	7283.55	28,103.34	7283.55
F	(kg/s)	1090.03	1090.03	1090.03	1090.03	1090.03
B_n	(kg/s)	696.09	696.09	696.09	696.09	696.09
TB_n	(°C)	32.93	32.87	35.50	32.82	34.40
TF^c	(°C)	26.10	26.10	30.23	27.29	30.72
TV^b	(°C)	31.93	31.87	34.50	31.82	33.40
$LMTD^c$	(°C)	5.88	5.82	6.15	5.15	4.65
$LMTD_1$	(°C)	9.65	9.60	9.12	9.49	9.66
$A^b{}_1$	(m^2)	454.42	433.20	540.67	450.27	553.14
A^e	(m^2)	37,049.76	36,986.01	39,805.546	37,004.75	38,068.99
A^p	(m^2)	12,030.85	12,085.60	10,523.55	11,177.86	9733.19
A^c	(m^2)	7623.53	7734.69	7674.88	9715.63	11,358.76
D^{ext}	(kg/s)	336.31	336.07	333.27	0.00	0.00
A	(m^2)	57,158.56	57,239.50	58,544.65	58,798.77	60,267.21
sA	(m^2/(kg/s of D))	145.09	145.30	148.61	149.26	152.99
PR	(kg/s of D/(kg/s of S))	5.27	5.27	5.27	5.27	5.27
CR	(kg/s of D/(kg/s of F))	0.36	0.36	0.36	0.36	0.36

[a] NUHTA_OP2 case but with an upper bound for the cooling water stream equal to this stream value for UHTA_OP1.

the flashing vapors ($V^{fb}{}_j + V^{fd}{}_j$) are higher than the vapor used in the preheaters ($V^p{}_j$), thus a part of the flashing vapor is used to evaporate the brine inside the effects; and for $j = N-1$, the amount of flashing vapors ($V^{fb}{}_j + V^{fd}{}_j$) is lower than the vapor used in the preheater ($V^p{}_j$), thus, a part of the vapor of brine evaporation ($V^b{}_j$) is used to preheat the incoming seawater in the preheater $J = N-1$, contrary to the conventional configuration. It can also be seen in Fig. 10 that V^p for preheaters is slightly higher for NUHTA_OP2 and 15% lower in the down condenser than for UHTA_OP1.

It is important to notice that, in the last effect, all distillate is extracted for NUHTA_OP2 before entering the flashing box (336.31) and therefore no vapor is produced by the flashing of distillate (the flashing box N is removed), while there is no extraction of distillate in the previous effects ($D^{ex}{}_j$ from $j = 1$ to $N-1$).

Finally, the influence of the different flow-patterns on the specific total heat transfer area (sA) was investigated and the results are illustrated in Fig. 11. As it was previously mentioned the highest and the lowest values are obtained for NUHTA_OP1 and NUHTA_OP2 respectively. The intermediate values correspond to the following flow-patterns: NUHTA_OP3: distillated extraction is not allowed but the flow-pattern for the vapor is now different in comparison to the conventional, and NUHTA_OP4: distillated extraction is allowed but considering the conventional flow-pattern for the vapor, as illustrated in Fig. 3. The comparison clearly shows how the specific total heat transfer area is increased when the novel configuration is restricted to the conventional arrangement.

The optimal solution for this case study corresponds to the novel configuration, with 5.16% improvement in total heat exchange area. The down-condenser is only used to condense the vapor formed in the last effect and not to preheat the feed seawater. The cooling water stream increases in a really significant value whereas the total heat transfer area in preheaters is higher than that required by the down-condenser. The heat transfer area in each evaporation

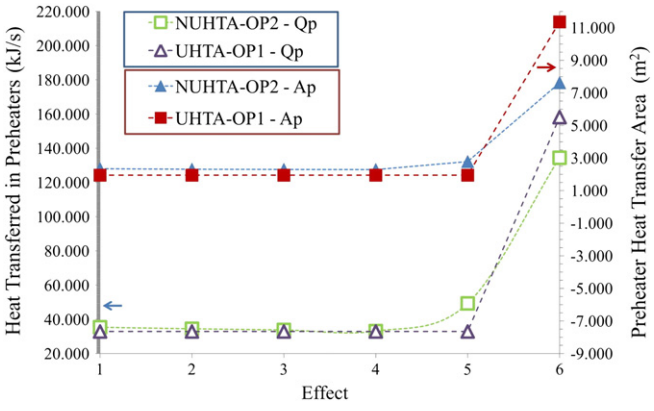

Fig. 7. Heat Transferred and HTA in each preheater (NUHTA_OP2 vs. UHTA_OP1).

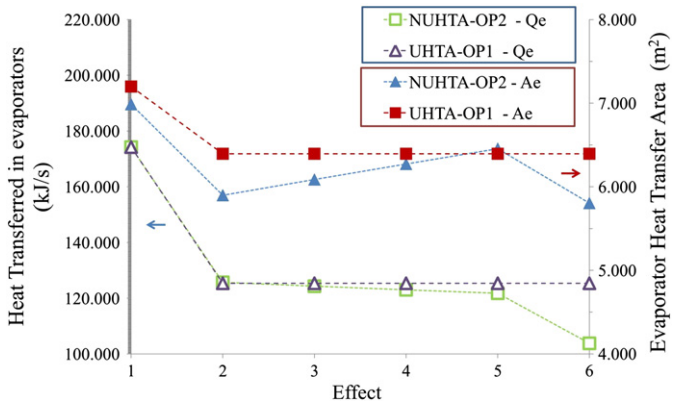

Fig. 6. Heat Transferred and HTA in each evaporation effect (NUHTA_OP2 vs. UHTA_OP1).

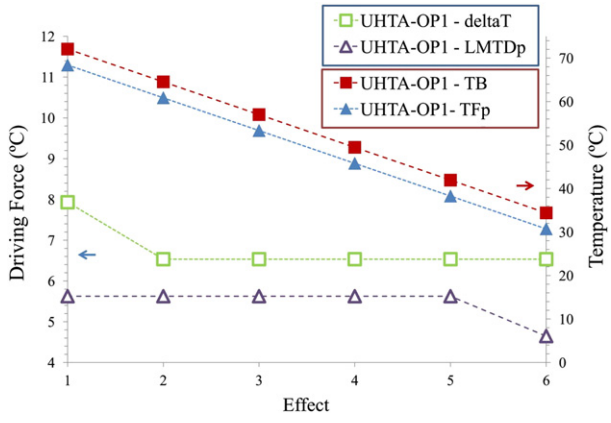

Fig. 8. Temperatures and driving forces in each effect for UHT-OP1.

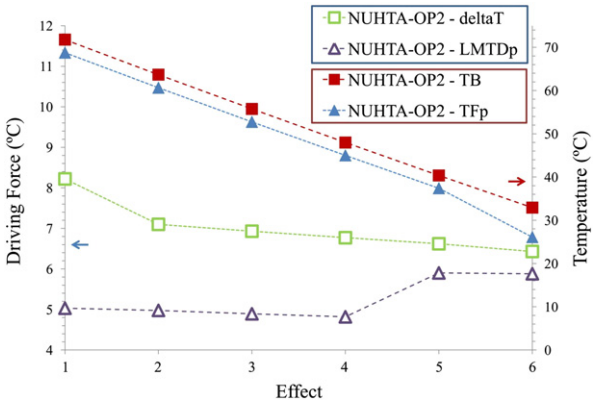

Fig. 9. Temperatures and driving forces in each effect for NUHT-OP2.

effect is lower, while the heat transfer area in each preheater, except in the down condenser, is slightly higher. The driving force profile for brine evaporation along the effects decreases smoothly and linearly, as well as the driving force profile for preheaters.

5.2.2. Sensitivity analysis

Table 10 reports the influence of each one of the model parameters (P_j) on the total heat transfer area (OF) for each one of the case studies analyzed in the previous section.

Similar qualitative conclusions observed previously, in case study 2, are also observed for each one of the proposed arrangement. An increment of 1% of Q or T^s or U or XB^{up}, the total heat transfer area decreases about 2.40, 1.20, 1.00 and 0.46, respectively. On the other hand, for an increment of D or λ the total heat transfer area increases about 2.30 or 2.95%, respectively. All parameters have similar influence in all cases, except for UHTA_OP2, where XF^{feed} becomes more sensitive than Cp and TF^{feed}. Despite this it should be mentioned, however, that the heat transfer area slightly varies with the increasing of XF^{feed}, Cp or TF^{feed}.

Regarding the influence of the TF^{feed} it is important to observe that in all cases the increment of this parameter leads to increase the total heat transfer area as occurred in case study 2.

5.2.3. Influence of the number of effects and heating utility temperature on the total heat transfer area and the total heat consumed

Finally, the influence of the number of effects and the steam medium temperature on the total heat transfer area and the total heat consumed was also investigated (Figs. 12 and 13). Table 11 lists the parameter values used for optimization.

As expected, the obtained Fig. 12 clearly shows that the specific total heat transfer area strongly depends on the number of effects (N) and the heating medium temperature (T^s). For any N, the sA decreases as T^s increases. On the other hand, for any steam temperature the sA increases as N increases; for instance, for $T^s = 60$ °C, the minimum specific total heat transfer for N = 12 is 105.75% higher than that required for N = 6. It should be noticed, however, that this difference significantly decreases as T^s increases, for example at $T^s =$ 100 °C the specific total heat transfer area for N = 12 is only 26.63% higher than that required for N = 6. These results would indicate that the best solution could be achieved with the minimum number of effects and the higher steam temperature.

Fig. 13 shows the optimal values of the specific total heat consumed, corresponding to the specific total heat transfer area shown in Fig. 12, for each value of T^s and N. In contrast to the heat transfer area behavior, the heat consumed increases as the number of effects decreases and the steam temperature increases. In summary, for any N and for each T^s, the lower heat transfer area, the higher heat consumed.

6. Conclusion

A deterministic and simplified NLP mathematical model to simulate and optimize the MEE system has been presented. Optimal profiles of temperature, salinity, heat transfer area and flow-rate along the MEE unit were simultaneously obtained in order to satisfy a given fresh water demand at minimum total heat transfer area. Once the proposed model was successfully verified with the literature, it was used to solve different optimization problems including the stream flow-patterns as optimization variables. The effect of the main process parameters on the optimal solutions has been also investigated. As a result, novel flow-patterns for the distillate and vapor streams were obtained which improve the process efficiency in comparison to the conventional arrangement. The total heat transfer area required for the novel flow-patterns was 5.16% lower than that required for the conventional one. The novel flow-patterns (distillate and vapor) allow allocating of the heat transfer area in a different way (varying the system temperatures, the driving forces and the flow-rates), resulting in a decrease of the total heat transfer area; however, the cooling water flow rate is significantly increased. Anyway, when the problem was solved with an upper bound for the cooling water stream, the total heat transfer area required was still lower than that required by the conventional case (2.86%). It was also observed that a non-uniform distribution of the heat transfer area along the MEE unit leads to increase the system efficiency in comparison to a uniform distribution; in some cases the improvement was significant.

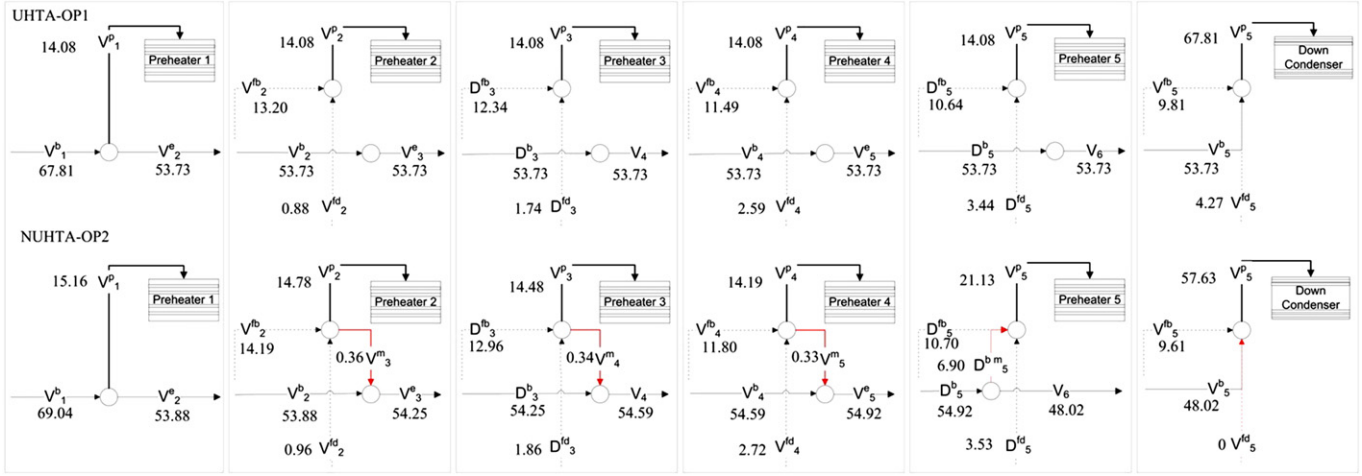

Fig. 10. Comparison of results for NUHTA-OP2 vs. UHTA-OP1.

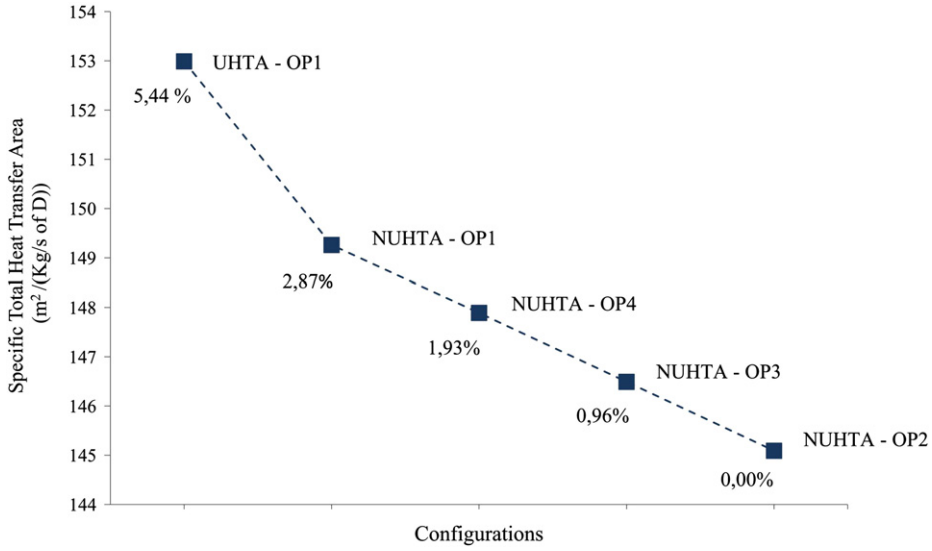

Fig. 11. Specific total heat transfer area for several configurations.

Table 10
Parameter sensitivity analysis — Relative marginal values (RMV).

Parameter	Unit	Value	RMV			
			Alternative flow-patterns		Conventional flow-patterns	
			NUHTA_OP2	UHTA_OP2	NUHTA_OP1	UHTA_OP1
λ	(°C)	2333.00	2.93	2.94	2.95	3.07
Q	(kJ/kg)	174,220.00	−2.40	−2.40	−2.33	−2.28
D	(ppm)	393.94	2.28	2.30	2.32	2.42
T^s	(kJ/s)	80.00	−1.18	−1.17	−1.18	−1.19
$U^e = U^p = U^c$	(kg/s)	3.00	−1.00	−1.00	−1.00	−1.00
XB^{up}	(°C)	72,000.00	−0.47	−0.48	−0.45	−0.45
TF^{feed}	(kJ/kg °C)	26.00	0.38	0.38	0.38	0.39
Cp	(°C)	4.00	0.36	0.36	0.36	0.36
XF^{feed}	(ppm)	45,978.90	0.32	0.63	0.31	0.30
BPE	(kW/m² °C)	1.00	0.15	0.15	0.16	0.16

Currently, the presented model is being extended in order to consider the number of effects as an optimization variable (discrete decision). The inclusion of the geometry (height, length and width), pressure drop and the minimization of the total cost (operating cost and investments) are also being considered. In fact, the convenience of each configuration discussed in this work considering the cost of each piece of equipment will be analyzed in detail. In addition, the dependence of the boiling point elevation, non-equilibrium allowance and the global heat transfer coefficient will also be included. Finally, the coupling of the MEE system and SOFT cells (Solid Oxide Fuel Cell) will be further investigated in detail.

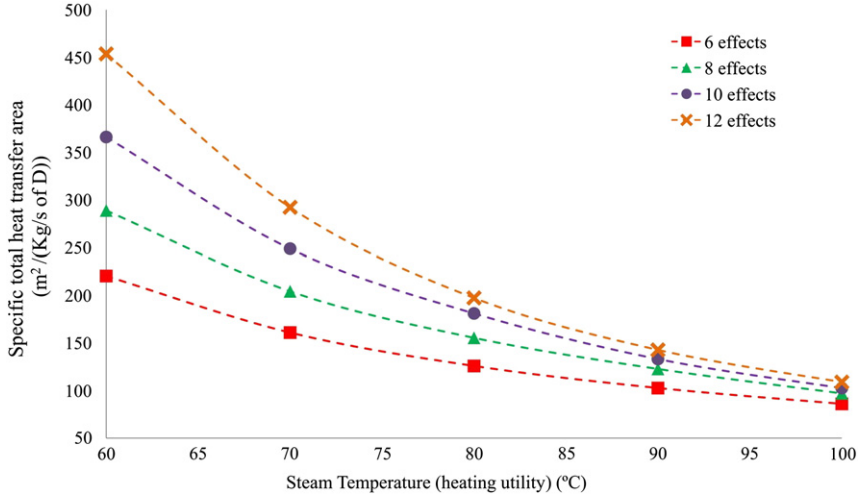

Fig. 12. Specific total heat transfer area and steam temperature vs. number of effect.

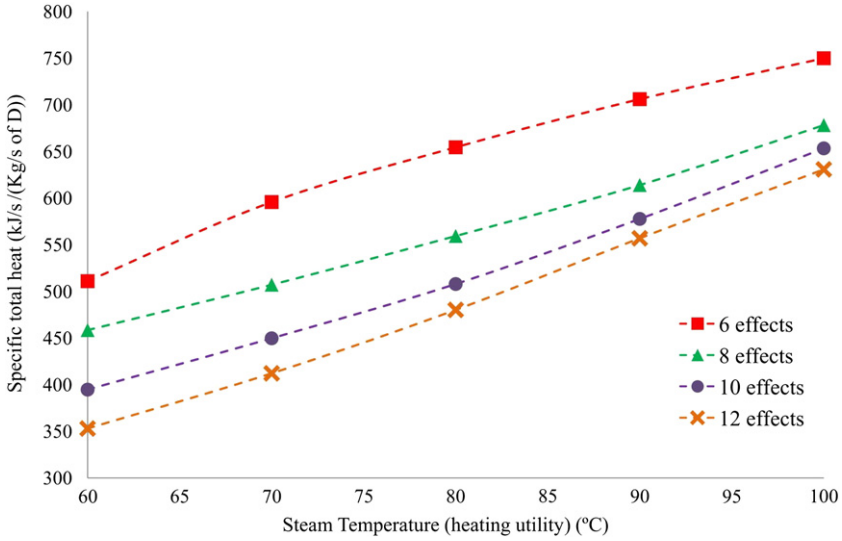

Fig. 13. Specific total heat and steam temperature vs. number of effect.

Nomenclature

A	Heat transfer surface area, m^2
B	Brine flow rate, kg/s
BPE	Boiling point elevation, °C
Cp	Specific heat at constant pressure of brine, kJ/kg °C
CR	Conversion Ratio, kg/s of D/(kg/s of F)
D	Mass flow rate of distillate, kg/s
F	Feed flow rate, kg/s
H	Water enthalpy, kJ/kg
LMTD	Logarithmic mean temperature difference, °C
N	Total number of effects
NEA	Non-equilibrium allowance, °C
PR	Performance Ratio, kg/s of D/(kg/s of S)
S	Heating steam, kg/s
sA	Specific total heat transfer area, m^2/(kg/s of D)
sWc	Specific cooling water rate, kg of F^c/s/(kg/s of D)
sQ	Specific total heat, kJ/s/(kg/s of D)
T	Stream temperature, °C
U	Overall heat transfer coefficients, kW/(m^2 °C)
Q	Heat flux, kJ/s
V	Mass flow rate of vapor, kg/s
X	Salt concentration, ppm
XB^{up}	Upper Bound of rejected brine salinity, ppm
λ	Latent heat, kJ/kg
ΔT	Temperature drop for effect
ΔT^p	Temperature drop for preheater

Superscript

b	Vapor formed by boiling
be	Vapor formed by boiling directed to the next evaporator
bm	Vapor formed by boiling mixed with flash streams
c	Cooling seawater
e	Evaporator
f	Feed flow rate in preheaters
fb	Vapor formed by flashing inside the effects
fd	Vapor formed by flashing inside the flashing boxes
ext	Extracted distillate flow rate
feed	Total feed seawater
fin	Flow in the flashing box
fot	Flow out the flashing box
m	Intermediate flow
p	Preheater
s	Heating steam

Subscripts

i: 1,2,…n Effect number

Table 11
Parameter values used for optimization.

Parameter	Unit	Value
Cp	(kJ/kg °C)	4.00
D	(kg/s)	393.94
S	(kg/s)	74.68
BPE	(°C)	1.00
λ	(kJ/kg)	2333.00
T^{feed}	(°C)	26.00
XF^{feed}	(ppm)	45,978.90
XB^{up}	(ppm)	72,000.00
$U^e = U^p = U^c$	(kW/m^2 °C)	3.00
N		6–12

Acknowledgment

Financial support obtained from the Consejo Nacional de Investigaciones Científicas y Técnicas (CONICET) and Agencia Nacional de Promoción Científica y Tecnológica (ANPCyT) is gratefully acknowledged.

References

[1] M. Al-Shammiri, M. Safar, Multi-effect distillation plants: state of the art, Desalination 126 (1999) 45–59.
[2] D.K. Akili, K.K. Ibrahim, W. Jong-Mihn, Advances in seawater desalination technologies, Desalination 221 (2008) 47–69.
[3] İ.H. Yılmaz, M.S. Söylemez, Design and computer simulation on multi-effect evaporation seawater desalination system using hybrid renewable energy sources in Turkey, Desalination 291 (2012) 23–40.
[4] H. Sayyaadi, A. Saffari, Thermoeconomic optimization of multi effect distillation desalination systems, Appl. Energy 87 (4) (2010) 1122–1133.
[5] A. Piacentino, E. Cardona, Advanced energetics of a Multiple Effects Evaporation (MEE) desalination plant: Part I: 2nd principle analysis by a zooming representation at single-effect level, Desalination 264 (1–2) (2010) 84–91.
[6] M. Khademi, M. Rahimpour, A. Jahanmiri, Simulation and optimization of a six-effect evaporator in a desalination process, Chem. Eng. Process. 48 (1) (2009) 339–347.

[7] N.M. Abdel-Jabbar, H.M. Qiblawey, F.S. Mjalli, H. Ettouney, Simulation of large capacity MSF brine circulation plants, Desalination 204 (1–3) (2007) 501–514.
[8] M.A. Darwish, F. Al-Juwayhel, H.K. Abdulraheim, Multi-effect boiling systems from an energy viewpoint, Desalination 194 (2006) 22–39.
[9] R. Kamali, A. Abbassi, S.S. Vanini, A simulation model and parametric study of MED–TVC process, Desalination 235 (1–3) (2009) 340–351.
[10] R. Kamali, S. Mohebinia, Experience of design and optimization of multi-effects desalination systems in Iran, Desalination 222 (1–3) (2008) 639–645.
[11] H.S. Aybar, Desalination system using waste heat of power plant, Desalination 166 (2004) 167–170.
[12] A. Jernqvist, M. Jernqvist, G. Aly, Simulation of thermal desalination processes, Desalination 134 (1–3) (2001) 187–193.
[13] J. VanAntwerp, A. Sykes, A.X. Si, Non Iterative Design of Multi Effect Evaporators using Excel ADD-INS, American Society for Engineering Education, 2009.
[14] N. Aly, A. El-Fiqi, Thermal performance of seawater desalination systems, Desalination 158 (2003) 127–142.
[15] H.T. El-Dessouky, H.M. Ettouney, F. Mandani, Performance of parallel feed multiple effect evaporation system for seawater desalination, Appl. Therm. Eng. 20 (2000) 1679–1706.
[16] A. Brooke, D. Kendrick, A. Meeraus, R. Raman, GAMS Language Guide, RELEASE 2.25, Version 92, GAMS Development Corporation, Washington D.C., 1997.
[17] H.T. El-Dessouky, H.M. Ettouney, Fundamentals of Salt Water Desalination, ELSEVIER SCIENCE B.V, Amsterdam, 2002.